

# UAV-BASED MULTI-SENSOR DATA FUSION FOR TIME-CRITICAL DISASTER RESPONSE

Oktay Baysal, Guoqing Zhou \*

Batten College of Engineering and Technology, Old Dominion University  
Norfolk, Virginia, 23529 Tel: (757) 683-3619; E-mail: gzhou@odu.edu

**KEY WORDS:** UAV, Data Fusion, Disaster Response, Video Flow, Real-time

## ABSTRACT:

We present a mathematical model for a UAV-based, multi-sensor data integration. As a background, we first discuss the design and the implementation of a low-cost civilian UAV system, including its field flight validation, system calibration, and mapping accuracy evaluation. Then, this photogrammetry-based mathematical model is developed. The field flight tests demonstrate that the designed low-cost UAV is capable of collecting clear and high-resolution video. The UAV can be controlled and navigated remotely and video stream and navigation data strings, including position and attitude, can be downlinked to the ground control station in real-time. The present multi-sensor, mathematical model reveal that the boresight matrix in a low-cost UAV system does not remain constant. This contradicts the practice in traditional airborne mapping systems where the boresight matrix is assumed to be a constant over an entire mission. Thus, to achieve a high-accurate mapping, EOPs of each video frame in a low-cost UAV mapping system have to be estimated. The present model can achieve a planimetric mapping accuracy using 1-2 pixels when compared with the USGS DOQ orthophoto.

## 1. INTRODUCTION

Forest fires may adversely impact more people in U.S.A than any other natural disaster. Nearly 1,000 structures and over 4 million acres of land are burned by wildfires annually (Kimball, 2003). In addition to the human and financial costs to the society, wildfires cause tremendous physical damages, and have notable environmental impacts. A reduction of wildfires demands large amounts of federal resources, costing up to \$1.6 billion per year, along with the lives of ten to twenty firefighters (Kimball, 2003). Therefore, the efforts of improving wildfire surveillance technology for mitigating disasters must continue.

Spaceborne-based and remotely sensed imagery has been a major data source for forest fire reconnaissance. Although the revisit cycle of useable satellites can be as good as one to three days, data collection at a revisit cycle of hours or decade minutes is increasingly required due to the requirement of fast-response to disasters (Zhou et al., 2009, 2002). Therefore, Unmanned Aerial Vehicles (UAVs) equipped with thermal infrared imaging technology and data telemetry to collect high-resolution video data, have been employed for forest fire surveillance in recent years (Wegener et al. 2002). The high-resolution video image, on the one hand, brings us clarity and details of the behaviour and characteristics of wildfire, on the other hand, presents new challenges in data processing. For example, how do we generate orthoimage from high-resolution UAV video images in forest fire areas at (near) real time? The orthoimage is critical geospatial data for wildfire experts, because: (1) it serves as a base map on which wildfire experts can add, register and compile other geospatial data; (2) it can be easily displayed as mosaiced products, quickly exploited to derive high-precision 3-D geolocations of objects within each video frame; (3) geometric measurement of wildfires (e.g.,

wildfire scopes, disaster areas), tree parameters (e.g., crown diameters, canopy closure) from orthoimages are more reliable than those from original perspective photographs since orthophotos theoretically are free of perspective distortion. The orthoimage will therefore be able to provide firefighters, wildfire analysts and decision-makers with greater situational awareness for wildfire behaviors, characteristics, and effects. The present paper reports the results of UAV-based multi-sensor data fusion for wild fire reconnaissance.

## 2. DESIGN AND IMPLEMENTATION OF UAV SYSTEM

In contrast to tactical or strategic ones used for military missions, these UAVs must carry highly reliable, accurate, but very expensive, and complicated instruments (Henri, 2004). The civilian UAV users have a strong demand for a low-cost, moderately functional, small airborne platform, varying in size, computerization and levels of autonomy (Moore et al., 2003). Therefore, how to develop such an economical UAV system, including hardware and software, for small private sectors and non-military government agencies to meet geospatial needs focusing on small areas of interest and that can be used for a broader array of mapping purposes, is key in designing and implementing our UAV platform.

For this reason, an end-to-end development for low-cost civilian UAV system including hardware and software has been implemented. The present paper reports only the research results pertaining to design and implementation of a small, lower-cost UAV system, and the multi-sensor data fusion. The real-time processing of the UAV-based video data and its evaluation for civilian applications in fast-response to time-critical disaster environments, such as wildfire surveillance,

---

\* Corresponding author. gzhou@odu.edu

analysis of the fire behaviour and characteristics, and decision-making for fire search and rescue (SAR) are all described in another paper.

### 2.1 UAV Platform

A 5-foot long and approximately 1.8-inches high UAV platform with a wingspan of 8 feet has been developed. Additional specifications are listed in Table 1. This UAV is made of sturdy plywood, balsa wood, and fiberglass materials. It features a proven versatile high-wing design and tail-dragger landing gear with excellent ground clearance that allows

operation from semi-improved surfaces. Generous flaps enable short rolling take-offs and slow flight. Its 1.5 hp, 2-stroke engine burns a commercial glow fuel mixed with gas. The fuel is held in an external tank just aft of the engine to avoid contamination with the payload and optical systems and to free up fuselage space (see Fig. 1). On-board, nickel-cadmium and lithium-polymer batteries power the UAV avionics, attitude reference, video camera, and telemetry systems. The UAV is constructed to break down into a few easy to handle components, which quickly pack into a medium size van, and are easily deployed, operated and maintained by a crew of three.

Power Plant	2 stroke, 1.5 hp	Wingspan:	8 ft	Fuel Capacity	16 oz.
Length × Height	5 × 1.5 ft	Cruise (Mission) Speed	45 mph	Endurance	50 minutes at cruise speed
Gross weight	22 lbs	Max Speed	65 mph	Payload	12 lbs
Operating Altitudes	600~2500 ft	Operating Range	~1.5-2.5 miles		

Table 1. Specifications of a low-cost civilian UAV platform

### 2.2 Multi-sensor Integration

In the UAV platform, the sensors are used to collect the video stream and provide UAV navigation. These sensors include GPS, attitude sensor (TCM2), and video camera. They have been integrated into a compact unit. An integrated sensor board has been developed for data flow downlinking.

#### Global Positioning System (GPS)

A GARMIN eTrex Vista Handheld GPS receiver is selected as the UAV positioning navigator. The eTrex Vista navigator has a 12 parallel-channel GPS receiver, which continuously tracks and uses up to 12 satellites to compute and update the position. The eTrex Vista combines a basemap of North and South America, with a barometric altimeter and electronic compass. The compass provides bearing information and the altimeter determines the UAV precise altitude.

#### Navigation Sensor (TCM2-20)

The TCM2-20 is selected as the UAV's attitude navigator. This sensor integrates a three-axis magneto-inductive magnetometer and a high-performance two-axis tilt sensor (inclinometer) in a package. It provides tilt compensated compass headings (azimuth, yaw, or bearing angle) and precise tilt angles relative to Earth's gravity (pitch and roll angle) for precise 3-axis orientation. This highly accurate inclinometer allows the microprocessor to mathematically correct for tilt. The magnetometers provide a very large dynamic range. The electronic gimbaling eliminates moving parts and provides information about the environment of pitch and roll angles, and three-dimensional magnetic field measurement. In addition, the many parameters of TCM2-20 are user programmable, including reporting units, sampling configurations, output damping. Data is output on a standard RS-232 serial interface with a simple text protocol that includes checksums.

#### Video Camera

A Topica Color TP 6001A CCD video camera was used to acquire the video stream at a nominal focal length of 8.5 mm with auto and preset manual focus, and program and manual exposure. The camera was installed in the UAV payload bay at a nadir looking direction. The video stream is recorded with a size of 720 (h) × 480 (v) pixel<sup>2</sup> and delivered in a MPEG-I format.

#### Integrated Sensor Board

An integrated sensor board was designed to sense, parse and combine the TCM2 attitude sensor and the GPS data streams into one usable data stream (for details, see Zhou, 2009). It is carried in the payload bay. In addition, the UTC (time) is designated to overlay onto the real-time video stream for time stamping purposes. The integrated sensor board consists of the TCM2 sensor, two IC Basic Stamps, one commercial video overlay board and associated circuit components such as resistors. The TCM2 attitude sensor has two modes of output; continuous output of heading, roll and pitch and on demand output at a baud rate of 9600. The Garmin GPS data streams are continuous 1 Hz data streams at a baud rate of 4800. Two IC Basic Stamps (mfg Parallax) were programmed and a simple asynchronous circuit was designed to provide one uniform data stream output from each of the Basic Stamps. One Basic Stamp parsed the GPS data streams and the other Basic Stamp parsed the TCM2 data streams. In addition, a spare Basic Stamp output pin was used to output the stored UTC (time) to the video overlay board.

### 2.3 Field Control Station

A field control station is set up in a mobile vehicle for providing command, control and data recording to and from the UAV platform. All data (GPS data, UAV position and attitude data, and video data) are transmitted to the ground receiver station via wireless communication, with real-time data processing in field for fast-response to rapidly evolving events. The van-mounted ground control equipment includes a 900-MHz receiver modems/antenna for the data stream and a 2.4-GHz microwave receiver/antenna for the video stream (Fig. 1a). Two commercial laptops and the necessary software are used for the data stream monitoring and the UAV position status systems. The data stream monitoring and recording are a commercial software system that runs on a Windows laptop (Fig. 1b). The UAV position status laptop uses commercial software that includes a Map Page that displays the current locations of the UAV and provides an interface for monitoring the UAV flying (route) status, GPS data stream status and UAV attitude. Power is provided to the systems through either a 12-volt DC battery bank or a 110-volt AC connection to an external power source (see Fig. 1b). For extended operations at remote sites, a small (1.8 KW) commercial generator supplies the AC power.

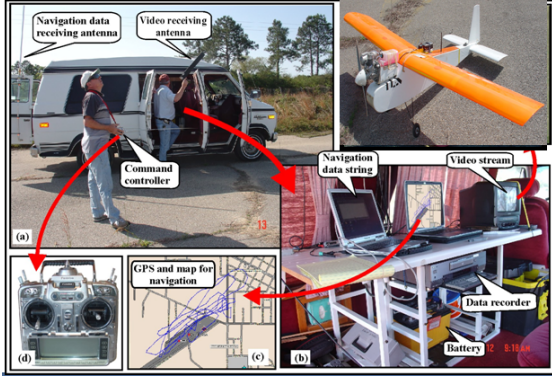


Fig 1. UAV ground control station and field data collection

### 3. MULTI-SENSOR DATA FUSION

For a UAV-based multi-sensor system, the relationship between the two navigation sensors and the video camera is given by the following equation (Skaloud, 1999):

$$r_G^M = r_{GPS}^M(t) + R_{Att}^M(t) \cdot [s_G \cdot R_C^{Att} \cdot r_g^C(t) + r_{GPS}^C] \quad (1)$$

where  $r_G^M$  is a vector containing a 3D object coordinate to be computed in the given mapping frame for a specific ground point  $G$ ;  $r_{GPS}^M(t)$  is a vector containing 3D coordinates of the GPS antenna phase center in the given mapping frame, which is determined by the GPS at a certain epoch ( $t$ );  $s_G$  is a scale factor between the camera frame and the mapping frame for a specific point  $G$ ;  $R_C^{Att}$  is the so-called *boresight matrix* (orientation offset) between the camera frame and the attitude sensor body frame, which is determined from system calibration;  $r_g^C(t)$  is a vector containing coordinates observed in the image frame for point  $g$ , which is captured and synchronized with GPS epoch ( $t$ ); and  $r_{GPS}^C$  is the vector of position offset between the GPS antenna geometric center and the camera lens center, which is usually determined by terrestrial measurements as part of the calibration process.  $R_{Att}^M(t)$  is a rotation matrix from the UAV attitude sensor body frame to the given mapping frame, which is determined by the TCM2 sensor at a certain epoch ( $t$ ), and is a function of the three attitude angles: *roll*, *pitch* and *yaw*.

So, the boresight calibration becomes the mathematical determination of matrix,  $R_C^{Att}$  using Eq. 1. This is usually solved by a least-squares adjustment on the basis of a number of well-distributed ground control points (GCPs). Once  $R_C^{Att}$  is determined, its value is assumed to be constant over the entire flight time of the airborne mapping system. Numerous investigators have addressed this calibration, such as, Schwarz et al. (1993); Cramer and Stallmann (2002), Jacobsen (2002), Csanyi and Toth (2003), Mostafa et al. (1998), and Grejiner-Brzezinska (1999).

In the present paper, we developed a new method which

simultaneously determines  $R_C^{Att}$  and the camera's interior orientation parameters, i.e., focal length ( $f$ ), principal point coordinates ( $x_0, y_0$ ), and lens distortion ( $p_l$ ). The details may be described as follows:

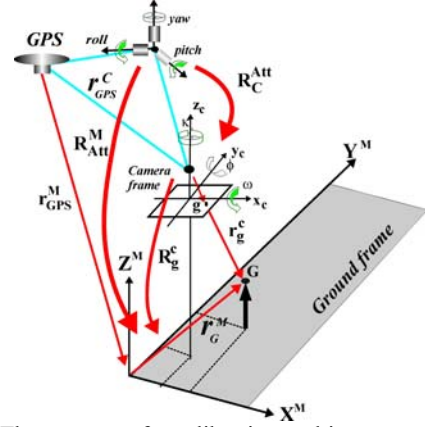


Fig 2. The geometry for calibrating multi-sensors, including video camera, GPS and attitude sensor

#### A) Determination of the Camera's IOPs

DLT (direct linear transformation) method, which was originally reported by Abdel-Aziz and Karara (1971), is used to calculate the initial interior orientation parameters (IOPs) and exterior orientation parameters (EOPs). This method requires a group of ground control points whose object space and image coordinates are already known. At this step, we have not considered the lens distortion because the calibrated IOPs and EOPs are taken as initial values in the rigorous calibration model.

#### B) Estimation of a Coarse Boresight Matrix

With the solved the EOPs, estimation of a coarse boresight matrix,  $R_C^{Att}$ , can be realized through multiplication of the attitude sensor orientation data derived from the onboard TCM2 sensor with the calculated three angular elements of the EOPs. The formula is given by,

$$R_C^{Att}(t) = [R_M^C(t) \cdot R_{Att}^M(t)]^T \quad (2)$$

where  $R_C^{Att}$  and  $R_{Att}^M$  are the same as in Eq. 1;  $R_M^C$  is a rotation matrix, which is a function of three rotation angles ( $\omega_1, \phi_1$ , and  $\kappa_1$ ) of a video frame.

#### C) Precise Estimation of the Boresight Matrix

With the coarse values computed, a rigorous calibration model, called *self-calibration bundle adjustment*, is employed to simultaneously solve the camera's interior orientation parameters (IOPs) and exterior orientation parameters (EOPs) of each video frame. In addition, because stereo camera calibration method can increase the reliability and accuracy of the calibrated parameters due to coplanar constraints (Betha et al., 1995; He, et al., 1993; Takahashi and Tomita, 1988; Thacker and Mayhew, 1991), a stereo pair of images constructed by the first and the second video frames is selected. The mathematical model, for any ground point,  $G$ , can be given as follows for the  $i^{\text{th}}$  video frame:

$$x_{g_1}^i - x_0 + \rho_1(x_{g_1}^i - x_0)r_1^2 = -f \frac{r_{11}^i(X_G - X_S^i) + r_{12}^i(Y_G - Y_S^i) + r_{13}^i(Z_G - Z_S^i)}{r_{31}^i(X_G - X_S^i) + r_{32}^i(Y_G - Y_S^i) + r_{33}^i(Z_G - Z_S^i)} = f_x^i \quad (3a)$$

$$y_{g_1}^i - y_0 + \rho_1(y_{g_1}^i - y_0)r_1^2 = -f \frac{r_{21}^i(X_G - X_S^i) + r_{22}^i(Y_G - Y_S^i) + r_{23}^i(Z_G - Z_S^i)}{r_{31}^i(X_G - X_S^i) + r_{32}^i(Y_G - Y_S^i) + r_{33}^i(Z_G - Z_S^i)} = f_y^i \quad (3b)$$

where

$r_{(i)}^2 = (x_{g_1}^i - x_0)^2 + (y_{g_1}^i - y_0)^2$  ( $i=1,2$ );  $(x_{g_1}^i, y_{g_1}^i)$  and  $(x_{g_2}^i, y_{g_2}^i)$  are the coordinates of the image point  $g_1$  and  $g_2$  in the  $i^{\text{th}}$  frames, respectively;  $(X_G, Y_G, Z_G)$  are the coordinates of the ground point,  $G$ ;  $(x_0, y_0, f, \rho_1)$  are the IOPs;  $r_{kl}^i$  ( $k=1,2,3; l=1,2,3$ ) are elements of the rotation matrix  $R$  for the first video frame (when  $i=1$ ) and the second video frame (when  $i=2$ ), which are a function of three rotation angles ( $\omega_1, \phi_1, \kappa_1$ ) and ( $\omega_2, \phi_2, \kappa_2$ ).

In this model, the unknown parameters contain the camera's IOPs,  $(x_0, y_0, f, \rho_1)$ , and the EOPs of the first and second video frames,  $(X_S^i, Y_S^i, Z_S^i, \omega^i, \phi^i, \kappa^i)$ , respectively. To solve these unknown parameters, Eqs. 3 must be linearized by using a Taylor series expansion including only the first-order terms.

With a number of high-quality, non-traditionally targeted GCPs obtained in Section 4.1, all unknown parameters in Eq. 3 can be solved using photogrammetric bundle adjustment methods. In the bundle adjustment model, 8 GCPs are employed and their imaged coordinates in the first and second images are also measured. The initial values of unknown parameters including  $(x_0, y_0, f, \rho_1)$ ,  $(X_S^1, Y_S^1, Z_S^1, \omega_1, \phi_1, \kappa_1)$  are provided by the above computation. Since the initial values of unknown parameters are provided, an iterative computation is carried out.

#### 4. EXPERIMENTAL RESULTS

	Roll ( $\omega$ )	Pitch ( $\phi$ )	Yaw ( $\kappa$ )	$X_0$	$Y_0$	$f$	$\rho_1$	$\sigma_0$ (pixel)
Onboard TCM2	0.07032	0.00245	1.08561	-	-	-	-	
DLT	-0.03407	0.00302	-1.09352				-	
Self-calibration	-0.015090	0.000021	-1.063786	360.20	240.32	790.54	-1.02e-7	1.92

Table 2. Results of IOPs and EOPs solved by different methods

Video Frames	Three angles obtained from TCM2 sensor (radian)	Three angles calculated from the photogrammetric model (radian)	Boresight matrix ( $R_C^{Att}$ ) calculated by $R_C^{Att} = [R_M^C \cdot R_{Att}^M]^T$ and angles ( $^\circ$ )	
Video frame #1	$roll = 0.070322$ $pitch = 0.002447$ $yaw = 1.085614$	$\phi = 0.000021$ $\omega = -0.015090$ $\kappa = -1.063786$	$\begin{pmatrix} -0.5470 & 0.8352 & 0.0575 \\ -0.8371 & -0.5465 & -0.0254 \\ 0.0102 & -0.0620 & 0.9980 \end{pmatrix}$	$\begin{matrix} -3.2955 \\ 1.4564 \\ 56.8605 \end{matrix}$
Video frame #2	$roll = 0.078880$ $pitch = 0.019850$ $yaw = 1.102259$	$\phi = -0.008159$ $\omega = -0.032069$ $\kappa = -0.853780$	$\begin{pmatrix} -0.4581 & 0.8867 & 0.0621 \\ -0.8887 & -0.4554 & -0.0529 \\ -0.0187 & -0.0794 & 0.9967 \end{pmatrix}$	$\begin{matrix} -3.5634 \\ 3.0335 \\ 62.8683 \end{matrix}$
Difference between two matrices			$\begin{pmatrix} -0.0890 & -0.0516 & -0.0046 \\ 0.0516 & -0.0911 & 0.0275 \\ 0.0288 & 0.0174 & 0.0014 \end{pmatrix}$	$\begin{matrix} 0.2678 \\ -1.5771 \\ -6.0078 \end{matrix}$

Table 3. Rotation angles with respect to the ground-based map frame and boresight matrix

#### 4.1 Test Field Establishment and Data Collection

A test field was established in Picayune, Mississippi, that is approximately 15 minutes north of NASA Stennis Space Center. This control field was about 4-miles long along N.W. and 3-miles wide along S.W. In this field, 21 non-traditional ground control points (GCPs) were collected using DGPS. These GCPs were located in the corners of sidewalk, or parking lot, crossroad, and curb end (see Fig. 2). The planimetric and vertical accuracy of the "GCPs" were at decimeter level.

The data collection was performed on April 3, 2005. The UAV and all the other hardware including computers, monitor, antennas, and the periphery equipment (e.g., cable), and the software developed within this project (Zhou, 2009) were transported to the test field via the field control station (see Fig. 1). After the UAV was assembled, its engine was fueled, all the instruments, such as antenna, computers, video recorder, battery, were set up. After testing the software system, the video data was collected.

#### 4.2 Accuracy Analysis of Multi-Sensor Data Fusion

The results from the abovementioned methods to calculate the IOPs and EOPs are listed in Table 2. Using these values of the IOPs and EOPs, the rotation matrix  $R_M^C$  is calculated via Eq. 3. Similarly, the  $R_{Att}^M$  can also be computed using the three orientation parameters ( $roll$ ,  $pitch$ , and  $yaw$ ) and the boresight matrix  $R_C^{Att}$  in Eq. 1. Their results are listed in Table 3.

As observed in Table 3, there are apparent differences that exist between the two boresight matrices corresponding to the two video frames at 0.2678°, -1.5771°, and -6.0078°, respectively. Further investigation of the boresight matrices corresponding to other video frames, it is also found that the boresight matrices corresponding to a series of frames varies continuously. These findings reveal an important fact that the boresight matrix for a low-cost UAV system can not remain a constant, as it typically is assumed so over an entire mission in a traditional airborne mapping system (Skaloud, 1999). This means that using a uniform boresight matrix for direct geo-referencing on the basis of onboard navigator is impractical for a low-cost UAV mapping system. Therefore, the exterior orientation parameters of each video frame in a low-cost UAV mapping system should

be estimated using traditional aerial triangulation techniques to obtain a precise boresight matrix for high-accuracy planimetric mapping.

### 4.3 Accuracy Evaluation of Planimetric Mapping

With the above presented method for the boresight matrix calculation, 2D planimetric mapping using the orthorectification method (Zhou et al., 2002) has been developed. In order to compare the accuracy, the 2D planimetry mapping using the attitude parameters from onboard attitude sensors, the boresight alignment is created as well. Both 2D planimetric maps are evaluated using five checkpoints. The results are listed in Table 4.

Accuracy relative to USGS DOQ	From self-calibration bundle adjustment	From boresight alignment	From GPS/TCM2
$\delta X$ (m)	0.17	10.46	44.04
$\delta Y$ (m)	0.25	10.33	56.26

Table 4. Accuracy evaluation of the 2D planimetric mapping derived using three orientation parameters, and  $\delta X = \sqrt{(X - X')^2/n}$ ,  $\delta Y = \sqrt{(Y - Y')^2/n}$ , where (X, Y) and (X', Y') are 2D coordinates planimetric mapping and the USGS DOQ, respectively.

## 5. CONCLUSIONS

We presented our results from the project entitled, "True Orthoimage Generation of High Resolution UAV (Unmanned Aerial Vehicle) Video for Forest Fire Surveillance." First, a low-cost civilian UAV system was designed and implemented. Then, a multi-sensor data fusion is developed using the photogrammetry model. Finally, the designed UAV system is calibrated using an established control field. The following were concluded from the experimental results:

The designed and implemented low-cost civilian UAV was capable of collecting video data focusing on specific areas of interest. The UAV could be controlled and navigated remotely by the ground control station, and video stream and navigation data strings could be real-time downlinked to the ground control station.

The proposed photogrammetry-based model for multi-sensor integration was able to simultaneously solve the video camera's IOPs (including lens distortion), and EOPs of video frames. The accuracy of 2D planimetric mapping could achieve 1.2 pixels, when compared with the planimetric maps derived by the other method.

With multi-sensor integration, it was found that the boresight matrix in a low-cost UAV system would not be able to remain a constant. Thus, the exterior orientation parameters of each video frame in a low-cost UAV mapping system had to be estimated to obtain a precise boresight matrix.

## ACKNOWLEDGMENT

This project was funded by the U.S. National Science Foundation under contract number of NSF 344521. The experimental work was conducted by post-doctoral researcher, Jun Wu.

## REFERENCES

- Abdel-Aziz, Y.I., and H.M. Karara, 1971. Direct linear transformation from comparator coordinates into object space coordinates in close-range photogrammetry. *Proceedings of the Symposium on Close-Range Photogrammetry* (pp. 1-18). Falls Church, VA, American Society of Photogrammetry.
- Bethea, M.D., J.A. Lock, F. Merat, and P. Crouser, 1997. Three-dimensional camera calibration technique for stereo imaging velocimetry experiments, *Optical Engineering*, vol. 36, no. 12, December, pp. 3445-3454.
- Cramer, M. and D. Stallmann, 2002. System Calibration for Direct Georeferencing. In *proceedings of International Society for Photogrammetry and Remote Sensing*, Graz, September 2002, Com. III, Part A, vol. 34, pp. 79-84.
- Csanyi, N., and C. Toth, 2003. Boresight Misalignment Determination of GPS/INS Supported Camera Systems Using a Single Ground Control Point, In *Proceedings of American Society of Photogrammetry and Remote Sensing (ASPRS) Annual Conference*, May 5-9 (CD-ROM).
- Grejner-Brzezinska, A. G., 1999. Direct Exterior Orientation of Airborne Imagery with GPS/INS System-Performance Analysis. *Journal of the Institute of Navigation*, 1999, vol. 46, no. 4, pp. 261-270.
- He, G., K. Novak, W. Feng, 1993, Stereo camera system calibration with relative orientation constraints, *Proceedings of the SPIE - The International Society for Optical Engineering*, vol. 1820, pp. 2-8.
- Henri, Eisenbeiss, 2004. A Mini Unmanned Aerial Vehicle (UAV): System Overview and Image Acquisition, *International Workshop on Processing and Visualization Using High-Resolution Imagery*, Pitsanulok, Thailand, November, 2004 (CD-ROM).

Jacobsen, K., 2002. Calibration Aspects in Direct Georeferencing of Frame Imagery. *Int. archive of ISPRS (International Society for Photogrammetry and Remote Sensing)*, Denver, Com. I, Part 1, vol. 34, pp. 82-89.

Kimball, P., 2003. Wildfires detection and monitoring through remote sensing, ASEN 5235 – Atmospheric Remote Sensing, <http://irina.eas.gatech.edu/ATO-Kimball-paper.pdf>.

Moore, M., C. Rizos, and J. Wang, 2003. Issues Concerning the Implementation of A Low Cost Attitude Solution for An Unmanned Airborne Vehicle (UAV), *In the 6th International Symposium on Satellite Navigation Technology Including Mobile Positioning & Location Services Melbourne*, Australia 22–25 July 2003 (CD-ROM).

Mostafa, M.R., K.P. Schwarz, and M.A., Chapman, 1998. Development and Testing of an Airborne Remote Sensing Multi-Sensor System, ISPRS Commission II, Symposium on Data Integration: Systems and Techniques, Cambridge, UK, July, Schwarz, K.P., M.E. Chapman, E. Cannon, and P. Gong, 1993. An Integrated INS/GPS Approach to the Georeferencing of Remotely Sensed Data. *Photogrammetric Engineering & Remote Sensing*, vol. 59, pp. 1667-1674.

Skaloud, J., 1999. Problems in Sensor Orientation by INS/DGPS in the Airborne Environment, *In Proceedings of ISPRS Workshop on Direct versus indirect methods of sensor orientation*, Barcelona, pp. 7-15.

Takahashi, H. and F. Tomita, 1988, Self-calibration of stereo cameras, 2nd International Conference on Computer Vision, pp. 123-128.

Zhou, G., 2009. Near real-time orthorectification and mapping of UAV-based video flow for time-critical event response, *IEEE Transactions on Geoscience and Remote Sensing*, vol. 47, no., 3, pp. 739-747.

Zhou, G. K. Jezek, and W. Wright, 2002. Orthorectifying 1960's declassified intelligence satellite photography (DISP) of Greenland, *IEEE Tran. on Geoscience and Remote Sensing*, vol. 40, no. 6, 2002, pp. 1247-1259.